JOURNAL OF APPLIED ELECTROCHEMISTRY 23 (1993) 316–321

Numerical simulation of electrochemical drilling

L. W. HOURNG, C. S. CHANG

Department of Mechanical Engineering, National Central University, Chung-Li, Taiwan, 32054

Received 4 November 1991; revised 27 July 1992

The purpose of the present paper is to describe the simulation of electrochemical drilling (ECD), which is generally affected by the electrical field and the flow field between two electrodes. A body-fitted transformation is applied to predict precisely the gradient of the electric potential field, and a bubbly-two-phase flow model is used to simulate the quasi-static electrochemical drilling process. The metal removal rate, determined by the variation of electric potential and the thermal-fluid properties, is then calculated. Numerical results agree well with experimental data. The void fraction is the most important factor in determining the electrolyte conductivity and the equilibrium shape of the workpiece. The overcut of the workpiece can be reduced by increasing the tool feed rate or decreasing the electrolyte flow flux. A bare bit type of tool, compared with coated tool and bare tool, can also diminish the overcut in ECD.

1. Introduction

Electrochemical machining (ECM) is a process of metal removal by high-rate anodic dissolution. The material to be machined is the anode and the tool, normally moving with a constant speed toward the workpiece, is the cathode. The electrolyte flows between the electrodes and carries away the metal dissolved from the anode. The advantage of such machining is that there is no wear on the tool; therefore, the cost and time for tool replacement is saved. Since machining is achieved by electrochemical reaction, hard materials can be machined as long as they are electrically conducting, and there is no residual stress on the workpiece.

However, ECM has not been widely used because of the inherently complex nature of electrochemical, thermal and hydrodynamic factors. Change of temperature and generation of gases in the electrode gap during machining cause a nonuniform distribution of local electrical resistance along the gap. As a consequence, the equilibrium shape of the workpiece is not congruent with the tool shape.

From the literature, research in predicting the workpiece shape may be classified into three categories. (i) By considering the effect of the *electrical field only*: analytic techniques include the cos θ method [1], analogue method [2] and the complex variables method [3]. However, they are basically limited to predict the equilibrium workpiece shape with simple geometries. The development of high speed digital computers has led to the application of numerical techniques such as the finite difference method [4, 5] and finite element method (FEM) [6, 7] in simulating the ECM process. Both methods are time consuming since mesh regeneration is necessary to compensate for the movement of the workpiece boundary during the ECM process. Another approach, known as the boundary element method (BEM) [8], has been found to be easy and accurate in predicting the workpiece shape. (ii) By considering the effect of the *flow field only*: the majority of the papers do not account for the effects of void fraction, varying temperature, etc., on the predicted anode profile [5, 9, 10]. Tipton [11] neglected void fraction and studied the effect of temperature on the shape of the electrode gap. Kawafune *et al.* [12], on the other hand, neglected temperature effects and studied the effect of void fraction. Thorpe and Zerkle [13] carried out an order of magnitude analysis and showed that void fraction and temperature effects are of the same order of magnitude. Later, Thorpe and Zerkle [14] proposed a one-dimensional, two-phase, fluid flow model and showed that most ECM can be treated as a quasi-static process. Hopenfeld and Cole [15] solved a quasi-static ECM process, however, the temperature effects were again ignored. (iii) By considering *both* the *electrical and flowfield effects*: Jain, Yogindra and Murugan [7] simulated an ECM process under the effects of the electric potential field and the flow field. However, in that paper the variation of electrolyte properties along the flow path is not obtained directly from the conservation equations but from some simplified or semi-empirical formulae, and the effects of the electrolyte flux and tool feed rate on the equilibrium workpiece shape are not discussed.

The purpose of the present paper, therefore, is to consider a more general simulation of ECM without ignoring any important effects. The electric potential field is solved by a finite difference method; however, a body-fitted transformation technique is used repeatedly to generate the mesh system during the process. The numerical error caused by the irregular boundaries can thus be reduced. A one-dimensional bubbly-two-phase flow model [14] is then used to simulate the flow field during electrochemical drilling. The equilibrium workpiece shapes obtained by the present method are compared with the experimental and other numerical results. Variations of the transport properties,

0021-891X

such as the electrolyte temperature, conductivity, and void fraction are investigated. Finally, the effects of operating parameters, such as the inlet flow rate of the electrolyte and the tool feed rate, on the machining are given an in-depth study.

2. Mathematical model of electrochemical machining

2.1. *The electric potential field*

Assuming properties of the electrolyte are homogeneous and neglecting the overpotential on the surfaces of the electrodes the distribution of the electric potential field between the electrodes is governed by Laplace's equation:

$$\frac{\partial^2 \phi}{\partial x^2} + \frac{\partial^2 \phi}{\partial y^2} = 0 \tag{1}$$

where ϕ is the electrical potential. For the electric potential field, the corresponding boundary conditions, as shown in Fig. 1, are as follows:

$$\left.\begin{array}{ll} \text{(i)} \ \phi = \phi_a & \text{along } \overline{AB}, \overline{BC} \text{ and } \overline{CD} \\ \text{(ii)} \ \phi = 0, & \text{along } \overline{HG}, \overline{GF} \\ \text{(iii)} \ \partial\phi/\partial n = 0, & \text{along } \overline{AH}, \overline{ED} \text{ and } \overline{EK} \\ \text{(iv)} \ \phi = 0 \text{ (bare bit tool), or} & \\ \quad \partial\phi/\partial n = 0 \text{ (coated tool),} & \text{along } \overline{FK}. \end{array}\right\} \tag{2}$$

2.2. *Kinematic relation*

In electrochemical machining, the variation of electrode gap y on position s is

$$\frac{\partial y}{\partial t} = V_a - V_c \tag{3}$$

where V_c is the local tool velocity, and V_a is the removal velocity of the anode in a direction normal to the tool surface. By Ohm's law and Faraday's law, Equation 3 can be written as

$$\frac{\partial y}{\partial t} = \frac{\varepsilon \lambda_a J}{\rho_a} - f_r \cos\theta \tag{4}$$

where λ_a is the electrochemical equivalent, ε the current flux, ρ_a the anode density, and f_r the feed rate of the cathode(tool). The current density, J, can be obtained by the gradient of the electrical potential, ϕ, as

$$J = k_e \frac{\partial \phi}{\partial n} \tag{5}$$

where n is the unit normal of the anode surface, and the electrolyte conductivity can be represented by [16]

$$k_e = k_0(1 - \alpha)^m[1 + \gamma(T_f - T_0)] \tag{6}$$

Here the zero subscript denotes condition at the entrance of the electrode gap, γ represents the conductance constant, and T_f is the electrolyte conduction temperature. The exponent m is a generalization of heterogeneous conduction mechanism and is taken to be 1.5 [16]. The void fraction is defined as

$$\alpha = \frac{y_g}{y} = \frac{y_g}{y_g + y_f} \tag{7}$$

where y_g and y_f represent the dimension occupied by the gas phase and the liquid phase, respectively.

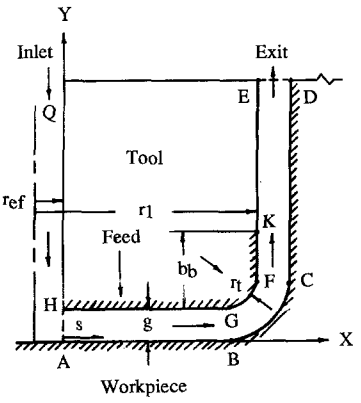

Fig. 1. A typical ECD configuration.

2.3. *Thermal and fluid equations*

In electrochemical drilling of a pre-drilled hole, the electrolyte flow is radially outward and can be assumed as one-dimensional. Since the amount of the dissolved metal is small, the flow is assumed to contain only two phases, namely, hydrogen gas and the electrolyte. The electrolyte is assumed to be incompressible while the hydrogen obeys the perfect gas law. The thermal conductivity and heat capacity of hydrogen are low compared to that of the electrolyte, hence, the transport of thermal energy is dominated by the electrolyte rather than the gas phase. Furthermore, the temperature difference between electrodes and the electrolyte is not large in practical situations, therefore, the heat flux transferred from electrodes to the electrolyte is negligible. Under these assumptions, the bubbly-two-phase model [14] can be applied, and the transport equations describing the flow can be derived as follows.

The continuity equation for the gas phase can be derived as

$$\frac{\partial}{\partial s}(\rho_g A_g V_g) + \frac{\partial}{\partial t}(\rho_g A_g) = \frac{A_g m_g}{y_g} \tag{8}$$

where A_g is the cross-section area and m_g is the mass flux of hydrogen gas generated at the interface and entering the gas control volume. The continuity equation for the liquid electrolyte phase is

$$\frac{\partial}{\partial s}(\rho_f A_f V_f) + \frac{\partial}{\partial t}(\rho_f A_f) = \frac{A_f(m_a - m_g)}{y_f} \tag{9}$$

where m_a is the mass flux of the anode. The momen-

tum equation for the liquid phase is

$$\rho_g y_g\left[\frac{\partial V_g}{\partial t}+\frac{\partial}{\partial s}\left(\frac{V_g^2}{2}\right)\right]+\rho_f y_f\left[\frac{\partial V_f}{\partial t}+\frac{\partial}{\partial s}\left(\frac{V_f^2}{2}\right)\right]$$
$$=-y\frac{\partial p_r}{\partial s}-(\tau_a+\tau_c)-m_a V_f-m_g(V_g-V_f) \tag{10}$$

where p_r is the pressure, τ_a and τ_c are the shear stresses acting on the anode and cathode. The energy equation is

$$V_f\frac{\partial T_f}{\partial s}+\frac{\partial T_f}{\partial t}$$
$$=\frac{H(T_a-T_f)+(m_a E/\varepsilon\lambda_a)+m_a(h_a-h_f)}{\rho_f y_f c_f} \tag{11}$$

where H is the convective heat transfer coefficient, T_a is the temperature of anode, h_f and h_g are the enthalpy of the electrolyte and gas, respectively, and c_f represents the specific heat capacity of the electrolyte. Finally, the equation of state for the gas phase is

$$p_r=\rho_g R_g T_f \tag{12}$$

On applying the analysis of order-of-magnitude, Thorpe and Zerkle [14] found that the transient behaviour of an ECM process is governed almost completely by the transient term $(\partial y/\partial t)$ in the kinematic equation, Equation 4. They also point out that the effect of the electrodes on the electrolyte heating is negligible, that is, the term $H(T_a-T_f)+m_a(h_a-h_f)$ on the right hand side of the energy equation, namely Equation 11 is zero. Furthermore, the term $m_a v_f+m_g(V_g-V_f)$ in the momentum equation, i.e. Equation 10 contributes little to the pressure gradient. The initial and boundary conditions required to solve the kinematic and conservation equations are the initial electrode gap $y_i(s)$, the electrolyte velocity at the entrance V_0, the exit pressure p_{re}, the electrolyte temperature at the entrance T_0. At the entrance, the void fraction is assumed to be zero because there is no gas.

3. Numerical procedure

The metal removal rate is a function of local current flux, which in turn depends on the electrical potential gradient along the workpiece. Since the shape of the workpiece is irregular and changes with time, a good grid distribution is needed for calculating the electrical potential gradient. In the body-fitted grid generation technique which we use here, a Poisson equation may be utilized to transform the system from the physical domain (x–y plane) to the rectangular computational domain (ξ–η plane). The transformation is [17, 18]

$$\left.\begin{aligned}\xi_{xx}+\xi_{yy}&=\Phi(\xi,\eta)(\xi_x^2+\xi_y^2)\\ \eta_{xx}+\eta_{yy}&=\Psi(\xi,\eta)(\eta_x^2+\eta_y^2)\end{aligned}\right\} \tag{13}$$

where Φ and Ψ are the control functions for the spacing of meshes. Interchanging the dependent and independent variables in Equation 13, we get

$$\left.\begin{aligned}\alpha(x_{\xi\xi}+\Phi x_\xi)-2\beta x_{\xi\eta}+\gamma(x_{\eta\eta}+\Psi x_\eta)&=0\\ \alpha(y_{\xi\xi}+\Phi y_\xi)-2\beta y_{\xi\eta}+\gamma(y_{\eta\eta}+\Psi y_\eta)&=0\end{aligned}\right\} \tag{14a}$$

where

$$\left.\begin{aligned}\alpha&=x_\eta^2+y_\eta^2\\ \beta&=x_\xi x_\eta+y_\xi y_\eta\\ \gamma&=x_\xi^2+y_\xi^2\end{aligned}\right\} \tag{14b}$$

Under the assumptions that transverse coordinate curves (ξ = constant) be locally orthogonal to the boundaries and the transverse coordinate curves be locally straight (i.e. have zero curvature) in the neighbourhood of the boundaries, the control functions along boundaries are as follows [17]:

$$\Phi(\xi,\eta)=-(x_\xi x_{\xi\xi}+y_\xi y_{\xi\xi})/(x_\xi^2+y_\xi^2) \tag{15a}$$

$$\Psi(\xi,\eta)=-(x_\eta x_{\eta\eta}+y_\eta y_{\eta\eta})/(x_\eta^2+y_\eta^2) \tag{15b}$$

The control functions for interior grid points are obtained by a linear interpolation between inner and outer boundaries. The governing equation of the electrical potential, namely Equation 1, is also transformed to and solved in the computational domain instead of in the physical domain. By utilizing Equations 14a and 15, Equation 1 can be rewritten as

$$\alpha(\phi_{\xi\xi}+\Phi\phi_\xi)-2\beta\phi_{\xi\eta}+\gamma(\phi_{\eta\eta}+\Psi\phi_\eta)=0 \tag{16}$$

where α, β and γ are the same as in Equation 14b. The numerical procedures are as follows:

(i) Input the initial shape of workpiece.
(ii) Calculate the control functions Φ and Ψ by Equations 15.
(iii) Calculate the grid distribution x and y by Equations 14.
(iv) Calculate the distribution of the electrical potential ϕ by Equation 16.
(v) Calculate the electrolyte velocity, pressure, void fraction, temperature, and gas density by solving five simultaneous differential equations, namely Equations 8–12.
(vi) Calculate the removal rate and the new shape of workpiece by Equation 4.

Steps (ii) to (vi) are repeated until the inter-gap reaches equilibrium.

In solving the electrical potential, Equation 16 is solved by a finite difference method with a successive over-relaxation to accelerate the convergence. To solve thermal and fluid equations, a finite difference method with forward difference for the time derivative and Euler implicit difference for the spatial derivative is applied. The trucation error is of the order of $[\Delta t^0, (\Delta s^0)^2]$. The iteration in each time step stops as the relative error of each variable is less than 10^{-3}. Calculation terminates as the shape of the workpiece reaches equilibrium, that is, the change of the workpiece shape in successive time steps is less than 10^{-2} in

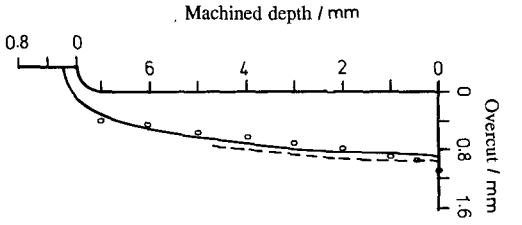

Fig. 2. Equilibrium workpiece shape in electrochemical drilling with a bare bit tool (Job no. 627). Key: (O) experimental data [6]; (– – –) numerical data [8]; (——) present calculation.

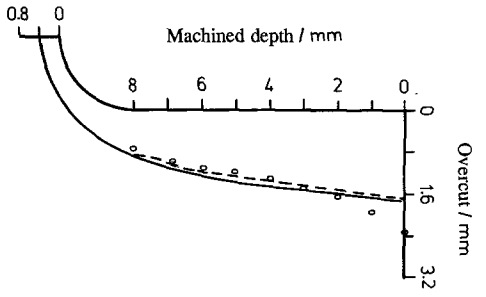

Fig. 3. Equilibrium workpiece shape in electrochemical drilling with a bare tool (Job no. 418). Key: (O) experimental data [6]; (– – –) numerical data [8]; (——) present calculation.

the front region. All calculations were performed on a HP-9000/835 workstation.

4. Results and discussion

The machining conditions and the electrolyte properties used for the present study are listed in Tables 1 and 2, respectively. Figure 2 shows the workpiece shape machined with a bare bit type of tool. Present results agree well, not only with the experimental data, [7] but also with the numerical data obtained from a finite element method [8]. The initial interelectrode gap for the present calculation is 1.0 mm, which is the same as that in [7] and [8]. By using a bare bit tool, the interelectrode gaps are generally large near the tool land, narrow near the tool tip, and vary linearly in between. The workpiece shape drilled by a bare tool is shown in Fig. 3. Present calculation and numerical results in [8] agree well with the experimental data, except in the tool land region, where the experiment yields a large overcut.

Figure 4 shows the numerical predictions of the workpiece shapes in electrochemical drilling by using different kinds of tools, namely, bare tool, coated tool

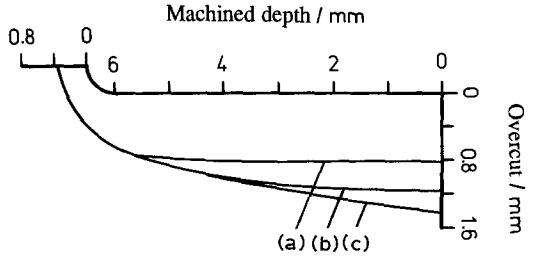

Fig. 4. Comparisons of the equilibrium workpiece shapes with different tools: (a) coated tool; (b) bare bit tool; (c) bare tool.

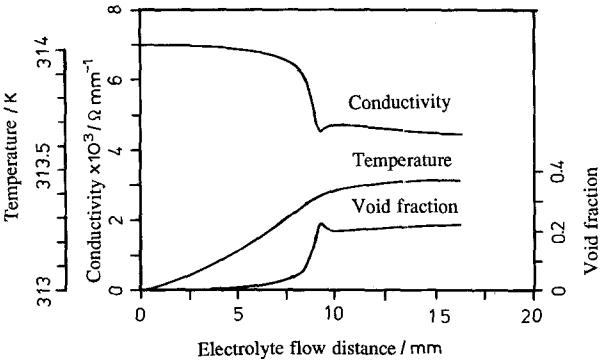

Fig. 5. Variation of the electrolyte temperature, conductivity, and void fraction along the stream path.

and bare bit tool. It indicates that the overcut can be reduced by the use of a coated tool. On the contrary, a bare tool produces a workpiece with large overcut. However, the coating in a coated tool will peel after a period of machining due to the effects of heat and electrolyte pressure. The frequent reconditioning of the coating makes the use of a coated tool uneconomical.

The distributions of the electrolyte temperature, void fraction, and the electrolyte conductivity in electrochemical machining with a bare bit tool are shown in Fig. 5. In the front region the electrical potential gradient is high, the Joule heating of electrochemical reaction accordingly increases the electrolyte temperature about 0.5 kelvin degrees. In the side region, the electrolyte temperature changes little. Hydrogen gas generated by electrochemical reaction is carried away by the electrolyte. Since the electrode gap decreases along the stream in the front and transition regions, the void fraction thus increases in the front region and reaches its maximum value in the transition region. In the side region, because the electrode gap increases gradually, the void fraction remains unchanged.

As can be seen from Equation 6, the electrolyte conductivity is proportional to the electrolyte tem-

Table 1. Working conditions of electrochemical machining

Job no.	627	725	418
Potential supplied/V	3.88	7.55	15.95
Electrolyte conductivity, $k_e/\Omega^{-1}\,mm^{-1}$	0.007	0.007	0.00532
Tool feed rate $10^3 f_r/mm\,s^{-1}$	3.70	3.70	5.71
Tool radius, r_1/mm	8.9	6.0	5.03
Tool corner radius, r_{tc}/mm	0.5	0.5	2.13
Height of the bare bit, b_b/mm	5.0	3.0	
Electrolyte flow flux, $Q/m^3\,min^{-1}$	5.37	5.37	5.37
Machining time, t/s	2400	2400	2400

Table 2. The properties of the electrolyte ($NaCl + H_2O$)

Temperature at the entrance: $T_{f0} = 313\,K$.
Density: $\rho_f = 1.06\,g\,cm^{-3}$
Specific heat capacity: $c_f = 4.18\,kJ\,kg^{-1}\,K^{-1}$
Viscosity: $\mu = 7.81 \times 10^{-3}\,g\,cm^{-1}\,s^{-1}$
Liquid-gas slip ratio: $\sigma = 1$
Electrochemical equivalent = 1

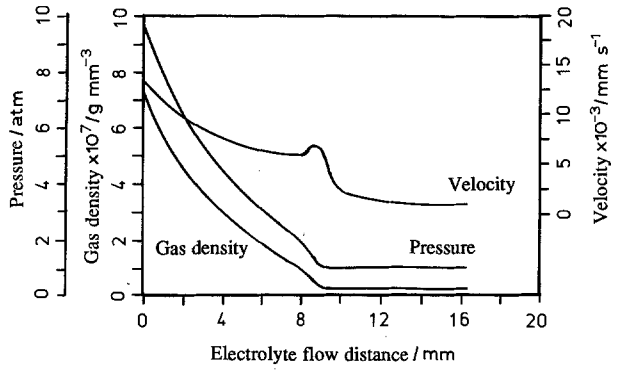

Fig. 6. Variation of pressure, gas density and velocity along the stream path.

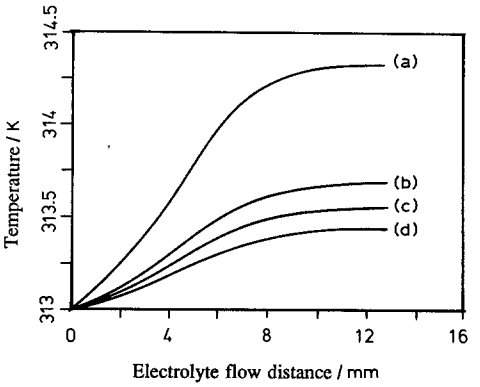

Fig. 8. Variation of electrolyte temperature with different electrolyte flow rates. Values of inlet flow flux rate: (a) 2.685, (b) 4.0275, (c) 5.37, and (d) 6.7125 $m^3 min^{-1}$.

perature and to the inverse of the void fraction. The increase in the electrolyte temperature along the stream tends to raise its conductivity, but the increase in the void fraction along the stream tends to reduce the electrolyte conductivity. However, the effect of void fraction on the electrolyte conductivity is more than that of temperature. Hence the electrolyte conductivity decreases along the flow path. The jump in conductivity and the jump in void fraction in the transition region are probably due to the rapid change of the geometry.

The variations of the electrolyte velocity, pressure and the gas density along the flow path are shown in Fig. 6. Since the workpiece is axially symmetric and the electrolyte flows radially outward from the centre of the frontal region, the electrolyte velocity decreases gradually (owing to the friction loss) along the stream path in the front area. In the transition region, the electrode gap becomes narrow abruptly, hence the electrolyte velocity increases rapidly in this region. In the side region, the interelectrode gap increases along the flow path so that the electrolyte velocity decreases again. Due to the effect of friction loss, the pressure decreases from the supplied pressure at the entrance to the atmosphere pressure at the exit. The gradient of pressure drop is high in the front and transition regions where the friction loss is high. The gas density, which is assumed to obey the perfect gas law, also decreases due to an increase in the electrolyte temperature and a reduction in electrolyte pressure.

The effect of the electrolyte flow flux on the workpiece shape is shown in Fig. 7. This indicates that the overcut enlarges as the electrolyte flow flux increases. This may be explained by the distributions of electrolyte temperature, void fraction and conductivity, as shown in Figs. 8 to 10. As the electrolyte flow flux increases, the heat generated by the current in the electrolyte between the electrodes is easily carried away, thus the temperature of the electrolyte becomes lower. The void fraction between the electrodes also becomes less as the electrolyte flow flux increases, since the hydrogen gas is removed rapidly by the electrolyte. It is worth noting that the void fraction changes rapidly in the transition region when a large electrolyte flow flux is applied. Choking may occur in the transition region if the electrolyte flux keeps increasing.

As mentioned before, the electrolyte conductivity increases as the electrolyte temperature rises or as the void fraction reduces. Since the effect of the void fraction is dominant in this case, the electrolyte conductivity becomes larger as the electrolyte flow flux increases. Due to the fact that the metal removal rate is proportional to the electrolyte conductivity, a large electrolyte flow flux thus results in a large metal removal rate or a short machining time. However, the accompanying overcut is also large as the electrolyte flux increases.

Figure 11 shows the effect of the tool feed rate on the workpiece shape. It indicates that the workpiece overcut becomes larger as the tool feed rate decreases. As the tool feed rate increases, the electrolyte gap decreases and the electrolyte velocity increases at the same electrolyte flow rate. The friction loss increases

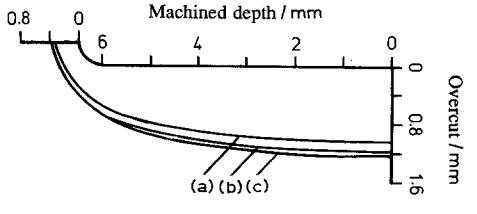

Fig. 7. Comparisons of equilibrium workpiece shapes with different electrolyte flow rates. Values of inlet flow flux rate: (a) 2.685, (b) 4.0275, and (c) 6.7125 $m^3 min^{-1}$.

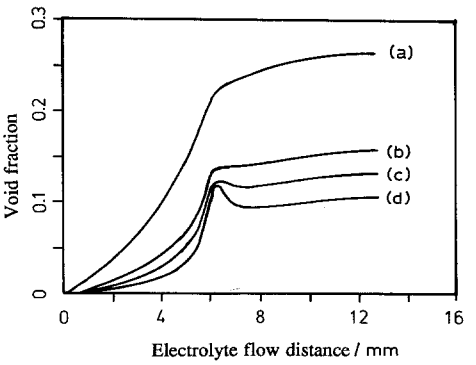

Fig. 9. Variation of void fraction with different electrolyte flow rates. Values of inlet flow flux rate: (a) 2.685, (b) 4.0275, (c) 5.37, and (d) 6.7125 $m^3 min^{-1}$.

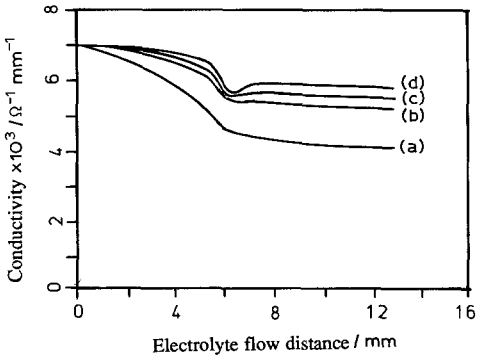

Fig. 10. Variation of electrolyte conductivity with different electrolyte flow rates. Values of inlet flow flux rate: (a) 2.685, (b) 4.0275, (c) 5.37, and (d) 6.7125 $m^3 min^{-1}$.

and the electrolyte temperature becomes higher. However, the hydrogen gas is easily carried away by the electrolyte, and the void fraction thus decreases. The electrolyte conductivity, which is affected primarily by the void fraction, is therefore less. It may thus be concluded that the metal removal rate as well as the workpiece overcut can be reduced by the increase of the tool feed rate. However, the tool feed rate can only be reduced to a certain value; beyond the limit of a certain value choking may occur [14] and the electric circuit between electrodes will be shortened.

5. Conclusions

The thermal and flow fields in electrochemical machining have been investigated, and several conclusions are made:

(i) Present calculations agree well with experimental data.

(ii) The electrolyte conductivity, as well as the electrode gap, are affected primarily by the void fraction, but not by the electrolyte temperature.

(iii) The overcut can be reduced by the use of a side-coated tool.

(iv) Metal removal rate, as well as the machining efficiency, can be enhanced by increasing the electrolyte flow flux. However, the overcut of the workpiece also becomes larger.

(v) The increase in the tool feed rate increases the void fraction and reduces the electrolyte conductivity; this results in a decrease in the workpiece overcut.

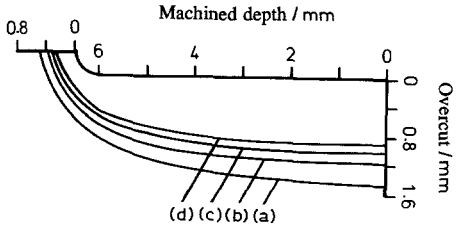

Fig. 11. Comparisons of equilibrium workpiece shapes with different tool feed rates. Values of tool feed rates: (a) 2.80×10^{-3}, (b) 3.7×10^{-3}, (c) 4.5×10^{-3}, and (d) 5.33×10^{-3} mm s^{-1}.

References

[1] A. L. Krylov, *Soviet Phys.* Doklady **13** (1968) 15.
[2] P. Lawrence, Ph.D. Thesis, Leicester University, UK (1977).
[3] D. E. Collett, R. C. Hewson-Brown and D. W. Windle, *J. Engineering Math.* **4** (1970) 29.
[4] V. K. Jain and P. C. Pandey, *Precision Engineering* **2** (1980) 195.
[5] M. B. Nanayakkare, Ph.D. Thesis, University of Strathclyde, UK (1977).
[6] V. K. Jain and P. C. Pandey, *Int. J. Mach, Tool Des. Res.* **22** (1982) 341.
[7] V. K. Jain, P. G. Yogindra and S. Murugan, *Int. J. Mach. Tools Manufact.* **27**(1), (1987) 113.
[8] O. H. Narayann, P. G. Yogindra and S. Murugan, *ibid.* **26**(3), (1980) 323.
[9] V. K. Jain and P. C. Pandey, *J. Engng. Indust.* **106** (1984) 55.
[10] O. H. Narayanan, S. Hinduja and C. F. Noble, *Int. J. Mach. Tool Des. Res.* **26** (1986) 323.
[11] H. Tipton, Proceedings of the 5th International Conference on Machine Tool Research, Birmingham, UK, Sept. (1964) 509.
[12] K. Kawafune, T. Mikoshiba, K. Noto and K. Hirata, *CIRP Ann.* **15** (1967) 65/1–65/13.
[13] J. F. Thorpe and R. D. Zerkle, *Report UCME-318-1*, Mechanical Engineering, University of Cincinnati, Cincinnati, OH, Dec. (1967).
[14] J. F. Thorpe and R. D. Zerkle, 'Fundamentals of Electrochemical Machining', (edited by C. L. Faust), Princeton, NJ (1971) p. 1.
[15] F. Hopenfeld and R. R. Cole, *J. Engng. Industry, ASME Trans.* **88** (1966) 455.
[16] F. F. Thorpe and R. D. Zerkle, *Int. J. Mach. Tool Des. and Res.* **9** (1969) 131.
[17] P. D. Thomas and J. F. Middlecoff, *AIAA J.* **18**(6), (1980) 652.
[18] J. F. Thompson, Z. U. A. Warsi and C. W. Mastin, 'Numerical Grid Generation', North-Holand, New York, NY (1985).